International Journal of General Medicine

Dovepress
Taylor & Francis Group

Open Access Full Text Article

ORIGINAL RESEARCH

Association of High Tumor-Stroma Ratio with Prostate Cancer Progression: Insights from Clinical and Genomic Data

Wenbo Xu[1,2], Qian Niu[3], Kun Zhao[1,2], Haozhi Zhao[1,2], Long Zhang[1,2], Wenxuan Li[1,2], Hong Yan[3], Zhilong Dong[1,2]

[1]Institute of Urology, Gansu Province Clinical Research Center for Urinary System Disease, The Second Hospital & Clinical Medical School, Lanzhou University, Lanzhou, Gansu, 730030, People's Republic of China; [2]Department of Urology, The Second Hospital & Clinical Medical School, Lanzhou University, Lanzhou, People's Republic of China; [3]Department of Pathology, The Second Hospital & Clinical Medical School, Lanzhou University, Lanzhou, Gansu, 730030, People's Republic of China

Correspondence: Hong Yan, Department of Pathology, The Second Hospital & Clinical Medical School, Lanzhou University, Lanzhou, Gansu, 730030, People's Republic of China, Email 363891078@qq.com; Zhilong Dong, Department of Urology, The Second Hospital & Clinical Medical School, Lanzhou University, Lanzhou, Gansu, 730030, People's Republic of China, Email dzl19780829@163.com

Background: Tumor stroma ratio (TSR) is a prognostic factor in various cancers, but its role in prostate adenocarcinoma (PRAD) remains unclear. This study investigates TSR's prognostic value in PRAD using clinicopathological data, bulk/single-cell RNA sequencing to explore tumor-stroma interactions and identify therapeutic targets.

Methods: Two PRAD cohorts (The Cancer Genome Atlas cohort, TCGA; Lanzhou University Second Hospital, LUSH) were analyzed for TSR associations with clinicopathological features and biochemical recurrence (BCR). TSR was assessed via digital image analysis and expert pathologist review. Publicly available bulk/single-cell RNA sequencing data were analyzed to identify TSR-associated genes and predict drug targets, pathways, and immunotherapy responses. Quantitative real-time PCR validated mRNA expression. In vitro assays assessed cell proliferation, growth, and migration, while in vivo xenograft assays validated BGN's role in promoting tumorigenesis.

Results: TSR significantly correlated with clinicopathological features (age, Gleason score, stage, seminal vesicle invasion, BCR) in both TCGA (n = 453) and LUSH (n = 320) cohorts. High TSR independently predicted BCR in multivariable Cox regression. High TSR was associated with copy number variations, differentially expressed miRNAs/transcription factors, and metabolic pathways. Predicted anti-cancer drug targets, like Ki8751, showed potential benefit in high-TSR patients. High TSR may correlate with poor immunotherapy response. Notably, downregulation of BGN in cancer-associated fibroblasts (CAFs) significantly suppressed cell proliferation, migration, and invasion in vitro, and in vivo xenograft assays confirmed that BGN downregulation inhibited tumor growth.

Conclusion: This study highlights TSR's prognostic significance in prostate cancer and its association with adverse clinical outcomes and complex tumor-stroma interactions, identifying BGN, a stromal cell-related gene, as a potential therapeutic target for CAFs. However, these findings are limited by the retrospective design, necessitating prospective validation.

Keywords: prostate cancer, tumor-stroma ratio, genomic, single-cell RNA sequencing, prognosis

Background

Prostate cancer (PCa) is the most prevalent and lethal male reproductive system cancer globally, with recent statistics showing its incidence and mortality rates among the top three.[1] Established risk factors for PCa include older age, family history, ethnicity, genetic mutations, and epigenetic modifications.[2,3] Prostate adenocarcinoma (PRAD) is the most common and aggressive histological subtype, originating from glandular epithelial cells.[4] Androgen receptor (AR) signaling, regulated by androgen hormones, is crucial for PCa initiation and progression.[5] Despite advances in early diagnosis and treatment, metastatic castration-resistant prostate cancer (CRPC) remains incurable and challenging to

Received: 31 December 2024
Accepted: 22 April 2025
Published: 20 May 2025

treat.[6] Therefore, identifying specific prognostic indicators is crucial for risk stratification and individualized treatment in prostate cancer. The tumor–node–metastasis (TNM) staging system, prostate-specific antigen (PSA) and Gleason score are key factors in PRAD management and prognosis.[7] However, these scoring systems lack consideration for tumor heterogeneity and biological characteristics, limiting their ability to provide comprehensive prognostic information for patients with diverse clinical outcomes. For example, PRAD patients with identical Gleason scores can exhibit distinct prognoses.[7] Therefore, identifying more comprehensive prognostic indicators is of paramount importance. The tumor stroma plays a crucial role in prostate cancer development, progression, and even therapeutic resistance.[8,9] Its primary functions include tissue structure formation and remodeling.[10] However, the clinical significance of tumor stroma in PRAD remains poorly defined and understood.

To investigate the tumor stroma, researchers initially focused on morphological assessment. Hematoxylin and eosin (H&E) staining enables rapid and convenient evaluation of tumor stroma ratio (TSR). This indicator has been highlighted as potential independent prognostic factor in other solid tumors, underscoring their significant clinical implications. Mesker et al (2007) were the first to demonstrate the prognostic significance of TSR in colorectal cancer, showing its independent predictive value for post-surgical outcomes.[11] Nowadays, the high TSR (stroma-rich) is established as an independent adverse prognostic factor in esophageal squamous cell carcinoma, bladder cancer, ovarian cancer, and overall survival (OS).[12–14] A meta-analysis of 14 studies involving 4238 patients with solid tumors confirmed that high TSR was associated with poor overall survival and disease-free survival.[15] These findings suggest TSR could serve as potential marker for evaluating tumor biology and predicting patient prognosis, reflecting the interplay between tumor cells and their microenvironment. While TSR's prognostic value is established in several solid tumors, its role in prostate cancer remains unclear due to limited standardized application and incompletely understood mechanisms. Therefore, a comprehensive evaluation of the correlation between TSR with clinicopathological features and prognosis in PRAD patients is warranted. Cancer-associated fibroblasts (CAFs) contribute to prostate cancer aggressiveness via extracellular matrix remodeling, growth factor secretion, and immune modulation. BGN, an extracellular matrix protein highly expressed in CAFs, promotes tumor growth and metastasis in other cancers, but its specific role in prostate cancer CAFs is less defined. Understanding TSR and stromal components like BGN may complement Gleason score, PSA, or genomic classifiers, providing additional prognostic information and therapeutic targets.

This study aims to elucidate the role of tumor stroma characteristics in PRAD progression, and to explore its potential as prognostic markers by combining clinicopathological information of prostate cancer patients in our hospital and TCGA database. In addition, by leveraging bulk RNA sequencing (buRNA-seq) and single-cell RNA sequencing (scRNA-seq), we revealed the interaction between tumor stroma and tumor microenvironment, identifying potential therapeutic targets. The flow chart for this study can be found in Figure 1.

Materials and Methods

Clinical Sample Analysis of TCGA and LUSH Cohorts

This study includes two cohorts: the Cancer Genome Atlas (TCGA) cohort and the Lanzhou University Second Hospital cohort (LUSH cohort). To evaluate the impact of clinical and molecular factors on biochemical recurrence (BCR) following radical prostatectomy, we employed Kaplan-Meier survival analysis and Cox proportional hazards regression. The TCGA cohort follows the publishing protocol of TCGA policies, while the LUSH cohort has been reviewed and approved by the Ethics Committee of Lanzhou University Second Hospital (with patient informed consent, Ethics Approval Number 2024A-1286). This study adheres to the Transparent Reporting of a Multivariable Prediction Model for Individual Prognosis or Diagnosis (TRIPOD) reporting guidelines[16] and is conducted in accordance with the Helsinki Declaration.[17] Patient selection criteria for the TCGA and LUSH cohorts can be found in Supplementary Figure 1.

TCGA Cohort

The TCGA cohort comprised patients diagnosed with PRAD via pathology and treated surgically, followed from 2012 to 2015, representing a Western patient population, in contrast to the LUSH cohort which consists of Chinese patients. Our search focused on prostate gland (Primary Site), slide images (Data Type), and diagnostic slides (Experimental Strategy).

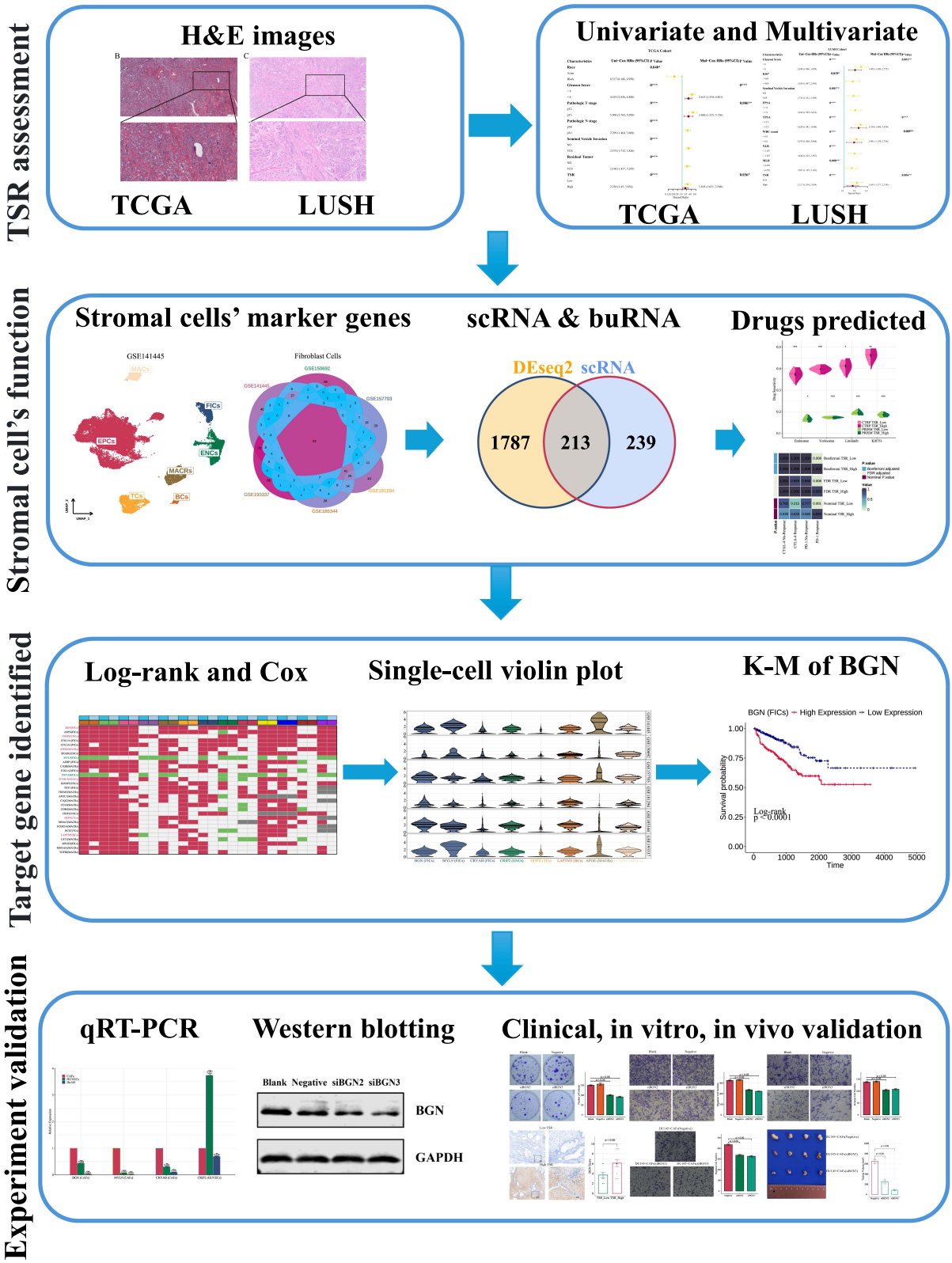

Figure 1 The flowchart of this study.

https://doi.org/10.2147/IJGM.S515066

Clinical and pathological reports were reviewed for age, race, Gleason score, pathologic T stage (pT), pathologic N stage (pN), seminal vesicle invasion, residual tumor, BCR and progression-free interval (PFI).

Lanzhou University Second Hospital Cohort

The LUSH cohort comprises 320 patients diagnosed with PRAD who underwent radical prostatectomy at Lanzhou University Second Hospital. Compared to the TCGA cohort, the LUSH cohort consists of a Chinese patient population with a more recent diagnosis period (2018–2024). Due to the shorter BCR-free survival in the Chinese patients (LUSH cohort) compared to the Western patients (TCGA cohort), along with substantial missing HE slide information before 2018 in the LUSH cohort, we limited the study to patients diagnosed between 2018 and 2024.[18] All patients were diagnosed with prostate cancer through biopsy before surgery, and none received neoadjuvant therapy before surgery, while all received standard postoperative systemic care. Clinical and pathological data, along with whole tissue H&E-stained slides (4 μm) were collected. Clinical and pathological data included age, body mass index (BMI), blood group, Gleason score, Ki67, seminal vesicle invasion, free prostate-specific antigen (FPSA), total prostate-specific antigen (TPSA), white blood cell (WBC) count, red blood cell (RBC) count, microscopic pyuria, microscopic hematuria, eosinophil-to-lymphocyte ratio (ELR), basophil-to-lymphocyte ratio (BLR), neutrophil-to-lymphocyte (NLR), and monocyte-to-lymphocyte ratio (MLR).

Immunohistochemistry slides (4 μm) from the time of diagnosis were also collected. These immunohistochemical markers included: androgen receptor (AR, prostate-specific biomarker), Ki67 (proliferation biomarker), prostate-specific antigen (PSA, prostate-specific biomarker), prostate-specific membrane antigen (PSMA, prostate-specific biomarker), cytokeratin high molecular weight (CK-H, epithelial biomarker), p63 (basal cell biomarker), P504s (prostate-specific biomarker), and synaptophysin (Syn, neuroendocrine cell biomarker). All patients were pathologically diagnosed with PRAD. Postoperative follow-up was conducted via telephone, with the cutoff date in September 2024. Follow-up information included postoperative examination results, adjuvant therapy details, BCR status and basis, and BCR time. Patients who died within one-month post-surgery or were lost to follow-up were excluded from the study.

Evaluation of Tumor Stroma Ratio in PRAD

The TSR was assessed in both TCGA and LUSH cohorts using digital image analysis. For the TCGA cohort, H&E-stained slides were downloaded from the GDC data portal and analyzed using ImageScope software. For the LUSH cohort, slides were digitally scanned and analyzed using the TissueFAXS PLUS system. Necrotic areas, normal tissue, and significant inflammation were excluded. A pathologist and a trained surgeon independently assessed TSR in representative areas of invasive tumor at 10x magnification. Discrepancies were resolved by a third experienced pathologist. Following published protocols.[19] TSR was determined by estimating the percentage of tumor cells and stroma within selected fields at 40x magnification. Patients were categorized into low-stroma (TSR $\leq$ 50%) and high-stroma (TSR > 50%) groups based on the lowest TSR value from at least three fields per patient.[20]

For a subset of samples, immunohistochemistry was performed. Pathological sections from 10 high-TSR and 10 low-TSR patients were incubated with a primary antibody against BGN (1:500 dilution) and then with a secondary antibody. Immunohistochemistry scoring was performed by the same team as TSR assessment.

In Silico Analysis of TSR-Associated Genomics Data

Single-Cell RNA Sequencing Data Collection and Preprocessing

Publicly scRNA-seq data (GSE141445, GSE150692, GSE157703, GSE181294, GSE185344, GSE193337) for PRAD were available through Gene Expression Omnibus (GEO, https://www.ncbi.nlm.nih.gov). For quality control, genes in fewer than 3 cells and cells with less than 200 genes were excluded from analysis. The gene-cell matrix was normalized using SCTransform after filtering. Dimensionality reduction was performed using principal component analysis (PCA) and uniform manifold approximation and projection (UMAP), enabling visualization of cell types. PCa cell types were annotated using manually curated marker genes from previously published prostate-related scRNA-seq data.[21–26] Differentially expressed genes (DEGs) were identified using Seurat's "FindAllMarkers" function.

Bulk Dataset Collection and Preprocessing

This study assembled nearly 2000 samples from 11 publicly available human bulk PCa datasets. RNA-sequencing data and clinical pathology data for a cohort of PRAD patients were obtained from the TCGA data portal. International Cancer Genome Consortium (ICGC) PRAD RNA-seq data was downloaded from the ICGC data portal (https://dcc.icgc.org/). RNA-seq data for the CPGEA cohort was downloaded from www.cpgea.com. The CITcohort bulk dataset was acquired from PCaDB (http://bioinfo.jialab-ucr.org/PCaDB/). Finally, bulk datasets from MSKCC, GSE54460, GSE70770, GSE94767, GSE116918, and GSE16560 were acquired from the GEO database.

Differential Gene Analysis, Enrichment, and Drug Targets

To identify genes associated with TSR, differential gene expression analysis was performed using the "limma" package in R. To analyze the biological functions and pathways associated with TSR, gene set enrichment analysis (GSEA) was conducted using GO, KEGG, and Hallmark gene sets. The Cancer Therapeutics Response Portal (CTRP) and Profiling Relative Inhibition Simultaneously in Mixtures (PRISM) datasets were used to predict potential drug targets for each TSR group. The Tumor Immune Dysfunction and Exclusion (TIDE) algorithm and subclass mapping were used to predict immunotherapy response between the risk groups.

Wet Lab Validation of BGN Function in CAFs

Cell Lines and Cell Culture

Prostate-CAFs and human umbilical vein endothelial cells (HUVECs) were cultured in DMEM medium (Gibco), while human prostate carcinoma DU145 cells were cultured in RPMI 1640 medium (Gibco). All cell lines were obtained from the Gansu Province Clinical Research Center for Urinary System Disease and were maintained in a humidified incubator at 37°C with 5% CO2. The culture medium was supplemented with 10% fetal bovine serum (HYCEZMBIO) and 1% penicillin/streptomycin. All cell lines were rigorously screened and confirmed to be mycoplasma-free prior to experimentation.

Quantitative Real-Time Quantitative PCR (qRT-PCR) Analysis

Total RNA was extracted using Trizol reagent (Yeasen, China) and reverse transcribed into cDNA using a high-capacity reverse transcription kit (ABclonal), following the manufacturer's instructions. qRT-PCR was performed using a CFX384 Real-Time PCR Detection System (Bio-Rad) with SYBR Green qRT-PCR reagent (ABclonal). The sequences of primers used for qRT-PCR were as follows: GAPDH (5′-3′ GGAGCGAGATCCCTCCAAAAT, 3′-5′ GGCTGTTGTCATACTTCTCATGG); BGN (5′-3′, TGACTGGCATCCCCAAAGAC, 3′-5′ GAGTAGCGAAGCA GGTCCTC); MYL9 (5′-3′, GGATGTGATTCGCAACGCCTTTG, 3′-5′ GCTTGGTATGGACGGGTGTGTG); CRYAB (5′-3′ CCTGAGTCCCTTCTACCTTCG, 3′-5′ CACATCTCCCAACACCTTAACTT); CRIP2 (5′-3′ ACTGATGCCTCCTCACCATC, 3′-5′ TGTTTGTGAGCCAACCAGAG).

siRNA Construction and Transfection

CAFs were seeded in six-well plates and subjected to siRNA transfection the following day.[27] CAFs were treated with 50nM of each siRNA for 6 hours, after which the media was changed. RNA expression levels were assessed by qRT-PCR 24 hours post-transfection, while protein expression levels were evaluated by Western blotting 48 hours post-transfection. Primer sequences purchased from TsingKe Biotech (Beijing, China). siBGN1, sense sequence (5'−3'), AGCUCUACAUCUCCAAGAA; antisense sequence, UUCUUGGAGAUGUAGAGCU. siBGN2, sense, CCACCUAGACCACAACAAA; antisense, UUUGUUGUGGUCUAGGUGG. siBGN3, sense, GCAUCAGCCUC UUCAACAA; antisense, UUGUUGAAGAGGCUGAUGC.

Cell Proliferation Assays

Cell Counting Kit-8 (CCK-8) assay (Yeasen) was utilized to quantified cell proliferation. Briefly, cells in a 96-well plate were treated with CCK-8 solution for 2 hours, and the cell viability post transfection was measured at 450 nm.

Plate Clone Formation Experiment

To ensure the formation of single-cell clones, cells were diluted and isolated into a 6-well plate after transfection. After 14-day incubation, the number of clones containing more than 50 cells was counted.

Cell Migration and Invasion Assays

The migration and invasion abilities of cells were assessed using transwell assays. For migration assays, cells were plated in serum-free DMEM in the upper chamber, while the lower chamber contained media supplemented with 10% FBS. For invasion assays, the upper chamber membrane was coated with Matrigel before cell seeding. Cells were incubated for 24 hours at 37°C in both assays. After the incubation period, the upper chamber cells were removed using a cotton swab, and the membrane was fixed in methanol and stained with crystal violet. The average number of migrated or invaded cells per field was determined by counting stained cells under a light microscope. Cell migration assays were performed using DU145 cells co-cultured with conditioned media from CAFs. CAFs were transfected with either negative control siRNA, siBGN2, or siBGN3. Following transfection, CAFs were cultured in serum-free media for 48 hours, and the conditioned media was collected.

Western Blotting

Western blotting analysis commences with sample preparation, involving the extraction of total protein from cells or tissues. The protein samples are then separated by SDS-PAGE electrophoresis and subsequently transferred to a PVDF membrane (IPVH00010, Millipore). Immunoreactions are then performed through blocking, primary antibody incubation (rabbit anti-BGN, 16409-1-AP, Proteintech), washing, and secondary antibody incubation (rabbit anti-GAPDH, 80570-1-RR, Proteintech). Finally, the target protein was visualized using the Odyssey CLx Imaging System (LI-COR) and images were captured.

Tumorigenicity Assay in Nude Mice

A total of 12 male BALB/c nude mice (4–5 weeks old, 17–19 g) were selected from Jicui Yaokang Biotechnology (Chengdu, China) for the experiment. All mice were housed in a specific pathogen-free (SPF) environment, maintained at a constant temperature of 23°C ± 2°C and humidity of 50% ± 5%. To establish a xenograft tumor model, nude mice were divided into three groups (n=4) and subcutaneously injected with DU145 cells mixed with CAFs transfected with either control siRNA, siBGN2, or siBGN3. Animal procedures complied with the National Institutes of Health (NIH) Guide for the Care and Use of Laboratory Animals and were approved by the Animal Ethics Committee of Lanzhou University Second Hospital (Ethical approval number: D2025-346).

Statistical Analysis

Statistical analysis and visualization were completed using R version 4.3.2 for Windows. Differences in clinicopathological characteristics between groups were determined using the Chi-square test, as appropriate. Correlations between continuous variables were assessed using two sample t -test (or Wilcoxon rank sum test). Survival analysis was conducted using the Kaplan-Meier method with Log rank test. Univariate and multivariate Cox regression analyses were performed to identify independent risk factors influencing BCR. A two-sided P-value less than 0.05 was considered statistically significant. Data analysis was conducted between September 2023 and September 2024.

Results

Clinical Characteristics Associated with TSR in Prostate Cancer

TSR Evaluation in TCGA and LUSH Cohort

A total of 453 patients were identified from the TCGA cohort after excluding one patient with non-primary PCa and 36 patients without survival information. After being evaluated by two pathology experts, 218 (48.12%) of the 453 analyzed samples were classified as low TSR, and 235 (51.88%) were classified as high TSR. The TSR-associated clinicopathological characteristics were summarized in Table 1. TSR was significantly associated with age, Gleason score, pathologic T stage, pathologic N stage, seminal vesicle invasion, residual tumor, BCR status and PFI status (all $P < 0.05$), but not with race. For the LUSH cohort, we finally included 320 patients with primary PCa, all of whom had undergone biopsy

Table 1 Comparisons of Characteristics Between Prostate Cancer Patients with High TSR and Those with Low TSR in TCGA Cohort

Characteristic	Overall (%)	Low TSR (%)	High TSR (%)	P Value[a]
Sample	453 (100)	218 (48.12)	235 (51.88)	
Age, median (IQR), year	61 (56, 66)	61 (55, 66)	62 (57, 66)	0.153
Age, year				0.03
41–57	149 (32.89)	83 (38.07)	66 (28.09)	
58–78	304 (67.11)	135 (61.93)	169 (71.91)	
Race				0.157
Asian	13 (2.87)	8 (3.67)	5 (2.13)	
Black	51 (11.26)	31 (14.22)	20 (8.51)	
White	376 (82.80)	174 (79.82)	202 (85.96)	
Unknown	13 (2.87)	5 (2.29)	8 (3.40)	
Gleason Score				< 0.001
< 8	266 (58.72)	150 (68.81)	116 (49.36)	
≥ 8	187 (41.28)	68 (31.19)	119 (50.64)	
Pathologic T stage				0.004
pT2	178 (39.29)	102 (46.79)	76 (32.34)	
pT3	264 (58.28)	113 (51.83)	151 (64.26)	
pT4	11 (2.43)	3 (1.38)	8 (3.40)	
Pathologic N stage				0.008
pN0	319 (70.64)	156 (71.56)	163 (69.36)	
pN1	73 (16.14)	25 (11.47)	48 (20.43)	
Unknown	61 (13.46)	37 (16.97)	24 (10.21)	
Seminal Vesicle Invasion				< 0.001
NO	321 (70.86)	173 (79.36)	148 (62.98)	
YES	132 (29.14)	45 (20.64)	87 (37.02)	
Residual Tumor				0.001
NO	286 (63.12)	155 (71.10)	131 (55.74)	
YES	141 (31.06)	50 (22.94)	91 (38.72)	
Unknown	26 (5.74)	13 (5.96)	13 (5.53)	
BCR status				< 0.001
NO	355 (78.37)	189 (86.70)	166 (70.64)	
YES	98 (21.63)	29 (13.30)	69 (29.36)	
PFI status				0.002
NO	365 (80.57)	189 (86.70)	176 (74.89)	
YES	88 (19.43)	29 (13.30)	59 (25.11)	

Notes: [a] Comparisons of categorical variables were conducted using Pearson $\chi 2$ tests, and the comparison of age between the groups was conducted using a *t* test with pooled variance.
Abbreviations: TSR, tumor–stroma ratio; TCGA, The Cancer Genome Atlas; IQR, interquartile range; BCR, biochemical recurrence; PFI, progression-free interval.

confirmation before surgery and underwent laparoscopic radical prostatectomy. Patients who had received endocrine therapy or open surgery before surgery were excluded. Of the 320 analyzed samples, 168 (52.50%) were classified as low TSR, and 152 (47.50%) were classified as high TSR. The TSR-associated clinicopathological characteristics were summarized in Table 2. TSR was significantly associated with age, Gleason score, seminal vesicle invasion, FPSA, TPSA, and BCR status (all $P < 0.05$), but not with BMI, blood group, Ki67, WBC count, RBC count, microscopic pyuria, microscopic hematuria, NLR, LMR, or PLR.

H&E Images in the TCGA and LUSH Cohorts and Immunohistochemistry in LUSH Cohort

Histological evaluation of TSR and immunohistochemistry were performed on TCGA and LUSH cohorts. Low and high TSR groups were defined based on H&E staining (Figure 2A–D). Immunohistochemical analysis of stromal cells, compared with prostate epithelial cells, revealed differential expression patterns in prostate cancer patients.

Table 2 Comparisons of Characteristics Between Prostate Cancer Patients with High TSR and Those with Low TSR in the LUSH Cohort

Characteristic	Overall (%)	Low TSR (%)	High TSR (%)	P Value[a]
Sample	320 (100)	168 (52.50)	152 (47.50)	
Age, median (IQR), year	68 (64, 73)	68 (64, 71)	69 (64, 74)	0.12
Age, year				0.045
43–69	188 (58.75)	108 (64.29)	80 (52.63)	
70–83	132 (41.25)	60 (35.71)	72 (47.37)	
BMI				0.626
18–23	134 (41.88)	73 (43.45)	61 (40.13)	
24–35	186 (58.13)	95 (56.55)	91 (59.87)	
Blood Group				0.237
A	87 (27.19)	48 (28.57)	39 (25.66)	
B	95 (29.69)	43 (25.60)	52 (34.21)	
AB	29 (9.06)	19 (11.31)	10 (6.58)	
O	109 (34.06)	58 (34.52)	51 (33.55)	
Gleason Score				< 0.001
< 8	150 (46.88)	95 (56.55)	55 (36.18)	
≥ 8	170 (53.12)	73 (43.45)	97 (63.82)	
Ki67				0.344
< 0.05	76 (23.75)	44 (26.19)	32 (21.05)	
≥ 0.05	244 (76.25)	124 (73.81)	120 (78.95)	
Seminal Vesicle Invasion				0.04
NO	227 (70.94)	128 (76.19)	99 (65.13)	
YES	93 (29.06)	40 (23.81)	53 (34.87)	
FPSA				0.021
< 1.9	203 (63.44)	117 (69.64)	86 (56.58)	
≥ 1.9	117 (36.56)	51 (30.36)	66 (43.42)	
TPSA				0.002
< 15.5	182 (56.88)	110 (65.48)	72 (34.52)	
≥ 15.5	138 (43.12)	58 (47.37)	80 (52.63)	
WBC count				1
< 8.9	257 (80.31)	135 (80.36)	122 (80.26)	
≥ 8.9	63 (19.69)	33 (19.64)	30 (19.74)	
RBC count				0.687
< 3.45	35 (10.94)	20 (11.90)	15 (9.87)	
≥ 3.45	285 (89.06)	148 (88.10)	137 (90.13)	
Microscopic Pyuria				0.713
Negative	124 (38.75)	63 (37.50)	61 (40.13)	
Positive	196 (61.25)	105 (62.50)	91 (59.87)	
Microscopic Hematuria				1
Negative	114 (35.62)	60 (35.71)	54 (35.53)	
Positive	206 (64.38)	108 (64.29)	98 (64.47)	
ELR				0.366
< 0.034	80 (25.00)	38 (22.62)	42 (27.63)	
≥ 0.034	240 (75.00)	130 (77.38)	110 (72.37)	
BLR				0.964
< 0.017	148 (46.25)	77 (45.83)	71 (46.71)	
≥ 0.017	172 (53.75)	91 (54.17)	81 (53.29)	
NLR				0.459
< 3.197	216 (67.50)	117 (69.64)	99 (65.13)	
≥ 3.197	104 (32.50)	51 (30.36)	53 (34.87)	

(*Continued*)

Table 2 (Continued).

Characteristic	Overall (%)	Low TSR (%)	High TSR (%)	P Value[a]
MLR				0.36
< 0.259	138 (43.12)	77 (45.83)	61 (40.13)	
≥ 0.259	182 (56.88)	91 (54.17)	91 (59.87)	
BCR status				< 0.001
NO	171 (53.44)	113 (67.26)	58 (38.16)	
YES	149 (46.56)	55 (32.74)	94 (61.84)	

Notes: [a] Comparisons of categorical variables were conducted using Pearson $\chi 2$ tests, and the comparison of age between the groups was conducted using a *t* test with pooled variance.

Abbreviations: TSR, tumor–stroma ratio; LUSH, Lanzhou University Second Hospital; IQR, interquartile range; BMI, body mass index; FPSA, free prostate-specific antigen; TPSA, total prostate-specific antigen; WBC, white blood cell; RBC, red blood cell; ELR, eosinophil-to-lymphocyte ratio; BLR, basophil-to-lymphocyte ratio; NLR, neutrophil-to-lymphocyte; MLR, monocyte-to-lymphocyte ratio; BCR, biochemical recurrence.

Immunohistochemical analysis revealed higher expression of AR, Ki67, PSA, and PSMA in stromal cells (Figure 2E–H). Conversely, lower expression of CK-H, p63, P504s, and Syn was observed in the stromal compartment (Figure 2I–L). Single-cell sequencing (Figure 2M) demonstrated a significant heterogeneity distribution of tumor and stromal cells across 53 prostate cancer patients.

Univariate and Multivariate Analysis and Survival Analysis in the TCGA and LUSH Cohort

To investigate prognostic factors for BCR, univariate and multivariate Cox regression analyses were conducted in the TCGA and LUSH cohort. Univariate Cox regression analysis identified seven clinicopathological characteristics—race, Gleason score, pathologic T stage, pathologic N stage, seminal vesicle invasion, residual tumor, and TSR—as being associated with prognosis in the TCGA cohort (Figure 3A). In parallel, univariate analysis of the LUSH cohort revealed that Gleason score, Ki67, seminal vesicle invasion, FPSA, TPSA, WBC count, NLR, MLR, and TSR were significantly associated with prognosis (Figure 3B). In multivariable Cox regression analyses, after adjusting for the aforementioned factors identified in the univariate analyses, we found that TSR remained a significant independent prognostic factor for BCR in both the TCGA and LUSH cohorts (Figure 3A and B). Next, Kaplan–Meier survival curves were constructed to evaluate the BCR of these patient subgroups, stratified by TSR (Figure 3C–E). It was observed that patients with low TSR had a significantly better prognosis ($P < 0.05$). Additionally, patients with low Ki67 expression also exhibited a more favorable prognosis ($P < 0.05$, Figure 3F). Furthermore, the receiver operating characteristic (ROC) curve based on TSR, and other risk factors was constructed to assess the ability of TSR to discriminate between patients with different prognoses (Figure 3G and H). The results suggest that TSR may possess sufficient specificity and sensitivity to be utilized in the clinical setting to identify patients at high risk of developing BCR.

Bioinformatic Analysis Reveals Genomics Alterations in High TSR Tumors

Single-Cell RNA Sequencing Landscape of PCa

Analysis of six scRNA-seq datasets encompassing 53 primary prostate cancer cases using Seurat package for data processing, normalization, and clustering revealed seven distinct cell types: epithelial, endothelial, fibroblast, T cells, B cells, macrophages, and mast cells (Figure 4A–F). The Venn diagrams results indicated marker genes for subpopulations of the aforementioned cell types (Figure 4G–L).

Identification And enrichment Analysis of TSR-Related Genes

To further elucidate the interrelationships between the distinct subpopulations within PCa, Spearman correlation analysis was subsequently performed (Figure 5A). The results demonstrated significant positive correlations among non-tumor cells within the prostate tumor microenvironment, except for mast cells. Notably, the high TSR group exhibited higher "Stroma Score", "Immune Score", and "Microenvironment Score", but lower "Tumor Purity" (Figure 5B–E). The intersection of differentially expressed genes between high and low TSR in TCGA and CAF-related genes identified

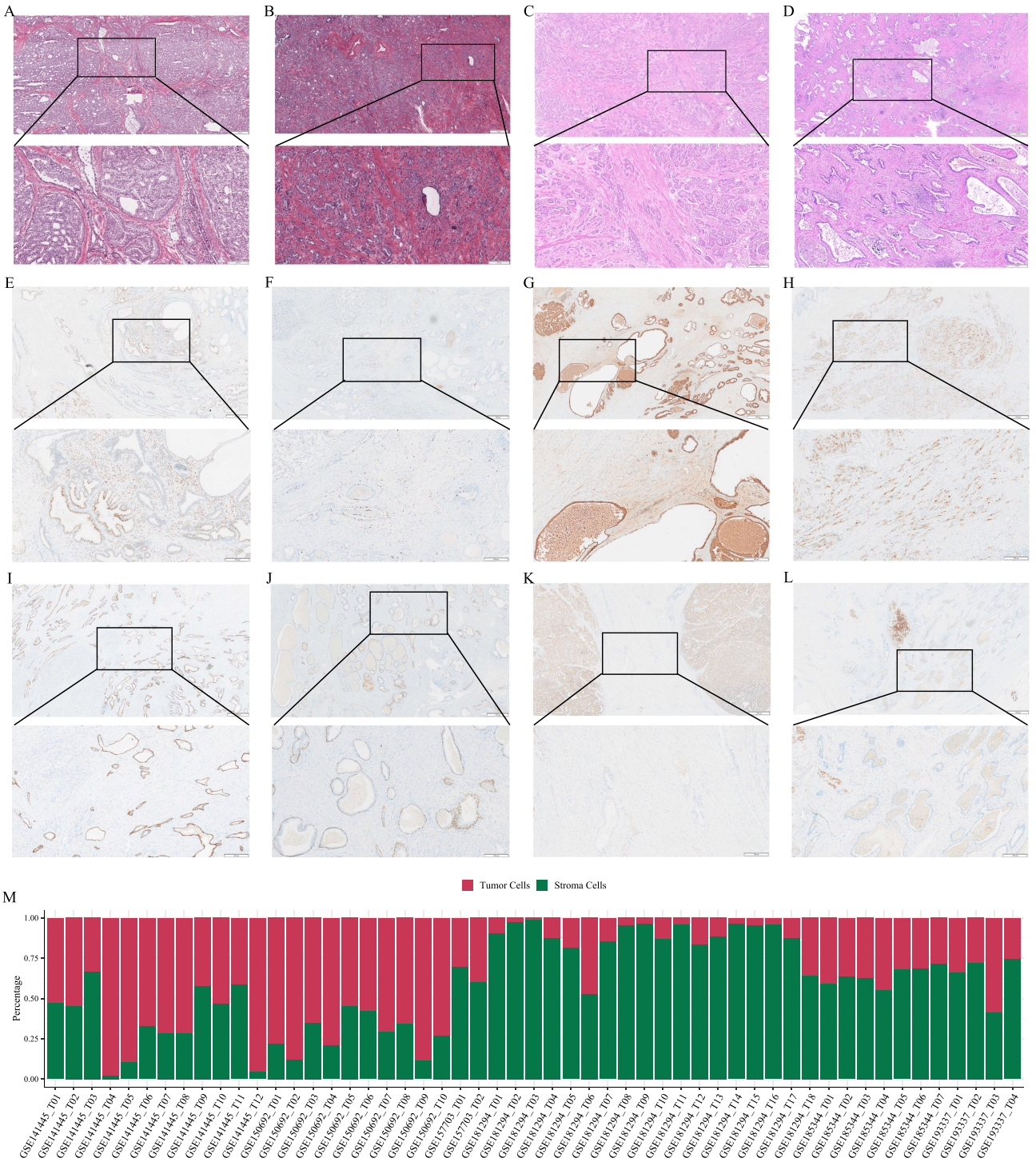

Figure 2 The histological evaluation of tumor stroma ratio (TSR) and immunohistochemistry. (**A**–**D**) The results of H&E images were used to divide TCGA and LUSH cohorts into low (**A** and **C**) and high (**B** and **D**) TSR groups. (**E**–**L**) Representative immunohistochemistry images of stromal cells from the LUSH cohort: (1) high expression of androgen receptor (AR, **E**), Ki67 (**F**), prostate-specific antigen (PSA, **G**), and prostate-specific membrane antigen (PSMA, **H**); (2) low expression of cytokeratin high molecular weight (CK-H, **I**), p63 (**J**), P504s (**K**), synaptophysin (Syn, **L**). (**M**) Single cell sequencing data demonstrated the spatial distribution of tumor and stromal cells in 53 prostate cancer patients.

by single-cell analysis yielded 213 genes (Figure 5F). Subsequently, we conducted GO, KEGG analysis, and hallmark pathway on these genes via GSVA package, a non-parametric unsupervised method for estimating pathway enrichment scores. GO analysis revealed distinct biological processes associated with low TSR (protein folding and stress response)

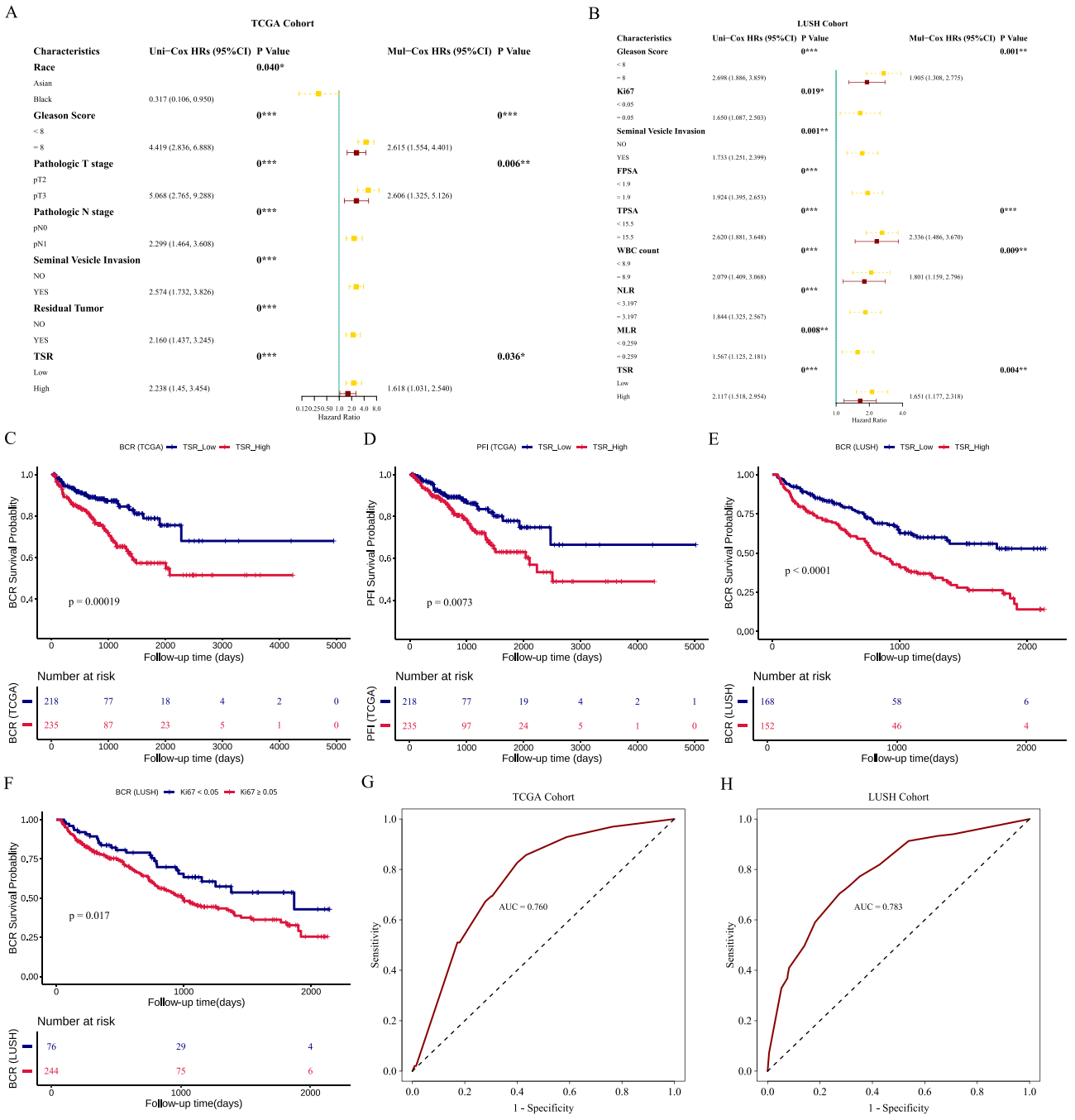

Figure 3 Univariate Cox and multivariate Cox regression analysis of tumor stroma ratio (TSR) groups and clinicopathologic factors in different cohorts. (**A** and **B**) Forest plot represents the results of univariate Cox and multivariate Cox regression analysis in The Cancer Genome Atlas (TCGA) and Lanzhou University Second Hospital (LUSH) cohorts. (**C** and **D**) Survival curves show biochemical recurrence (BCR) and progression-free interval (PFI) rates of prostate cancer patients with low or high TSR from the TCGA cohort. (**E** and **F**) Survival curves show BCR of prostate cancer patients with low or high TSR and Ki67 from the LUSH cohort. (**G**) The receiver operating characteristic (ROC) curves of risk factors in TCGA cohort. (**H**) The ROC curves of risk factors in LUSH cohort. *p < 0.05, **p < 0.01, ***p < 0.001.

and high TSR (immune cell activation and regulation) groups (Figure 5G). KEGG analysis identified distinct metabolic pathways (N-glycan biosynthesis, cholesterol biosynthesis, autophagy) in low TSR and immune signaling pathways (complement and coagulation cascades, cytokine JAK-STAT signaling) in high TSR groups (Figure 5H). Hallmark pathway analysis revealed distinct cellular processes (androgen signaling, fatty acid metabolism, cholesterol homeostasis) in low TSR and immune-related pathways (KRAS signaling up, angiogenesis, complement system) in high TSR groups (Figure 5I).

https://doi.org/10.2147/IJGM.S515066

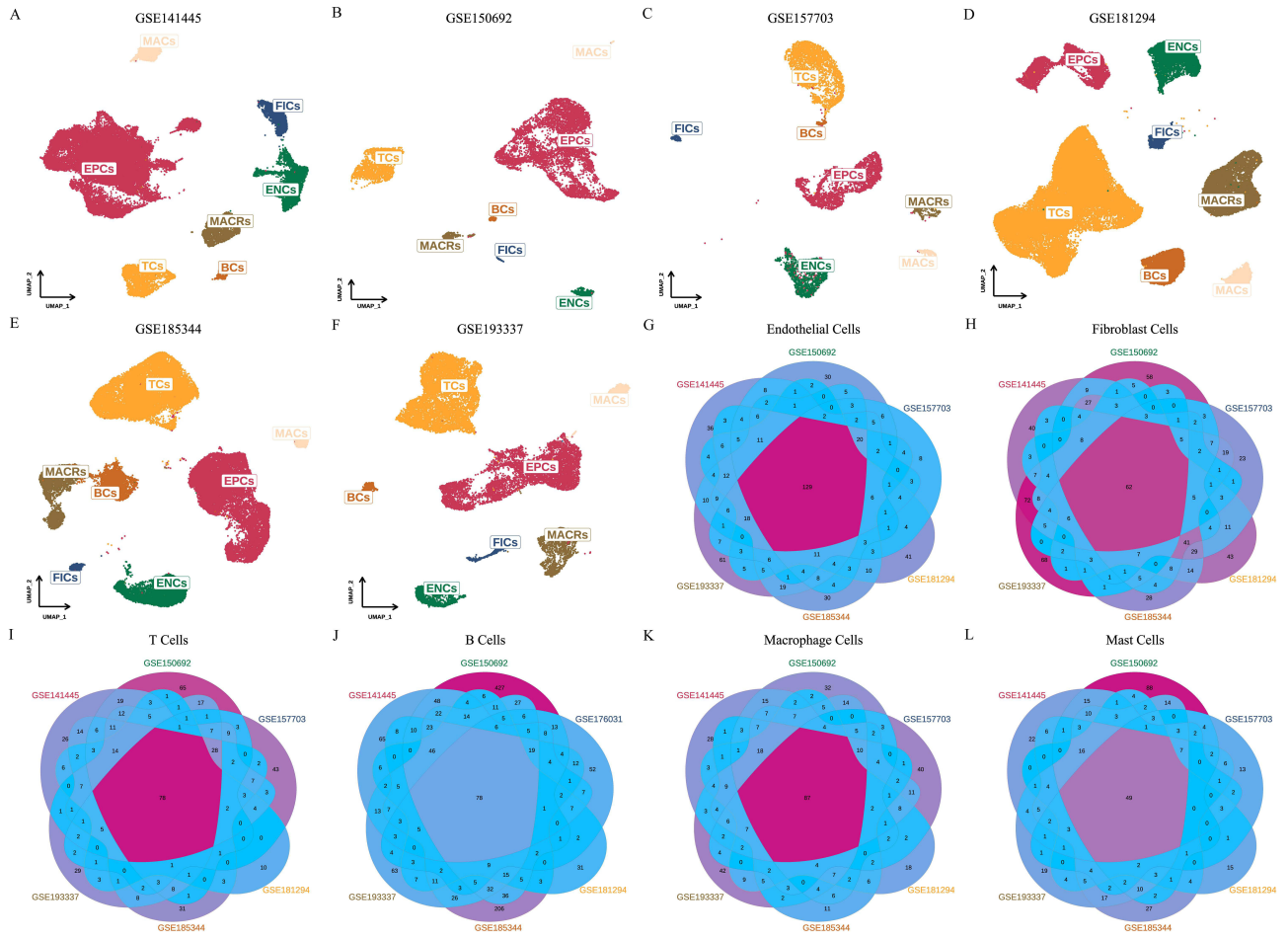

Figure 4 Single-cell landscape of prostate cancer. (**A**–**F**) Uniform Manifold Approximation and Projection (UMAP) plots of six datasets (GSE141445, GSE150692, GSE157703, GSE181294, GSE185344, GSE193337) showed single cells colored by the seven cell types (EPCs: epithelial cells; ENCs: endothelial cells; FICs: fibroblast cells; TCs: T cells; BCs: B cells; MACRs: macrophage cells; MACs: mast cells). (**G**–**L**) Numbers of overlapping gene pairs in the marker genes of six cell types.

We found that both high and low TSR groups exhibited copy number variations, but the high TSR group displayed a greater number of variations. (Figure 6A). We also demonstrated the most significantly differentially expressed miRNAs, transcription factors and metabolic pathways between high and low TSR groups in a heatmap (Figure 6B). In addition, we predicted potential anti-cancer drugs based on the CTRP and PRISM databases. Among the four drugs screened (Entinostat, Vorinostat, Linifanib, Ki8751), Ki8751 may have an advantage in targeting patients with high TSR scores (Figure 6C). At the same time, we found that patients with high TSR scores may have a poor response to immunotherapy (Figure 6D and E).

Identify Prognostic Key Genes in Each Subgroup

Univariate Cox regression and Kaplan-Meier survival analyses were performed in 13 PCa datasets to investigate the association between the expression of subgroup-associated genes and PFI, BCR, MET, and OS (Figure 7A). The top 30 genes with the strongest associations were presented, and Kaplan-Meier survival curves were used to visualize the prognostic relevance of these genes in each subgroup (Figure 7B–I). Meanwhile, the expression of these subgroup-associated genes was visualized in six single-cell datasets (Figure 7J).

BGN Regulates CAFs Growth in vitro and Promotes Tumor Growth in vivo

The expression of BGN, MYL9, CRYAB, and CRIP2 was validated at the cellular level (epithelial cells, FICs, ENCs) using PCR (Figure 8A), confirming our previous data analysis. The knockdown efficiency of BGN in CAFs was validated using PCR and Western blot (Figure 8B and C), demonstrating that siBGN2 and siBGN3 achieved the expected

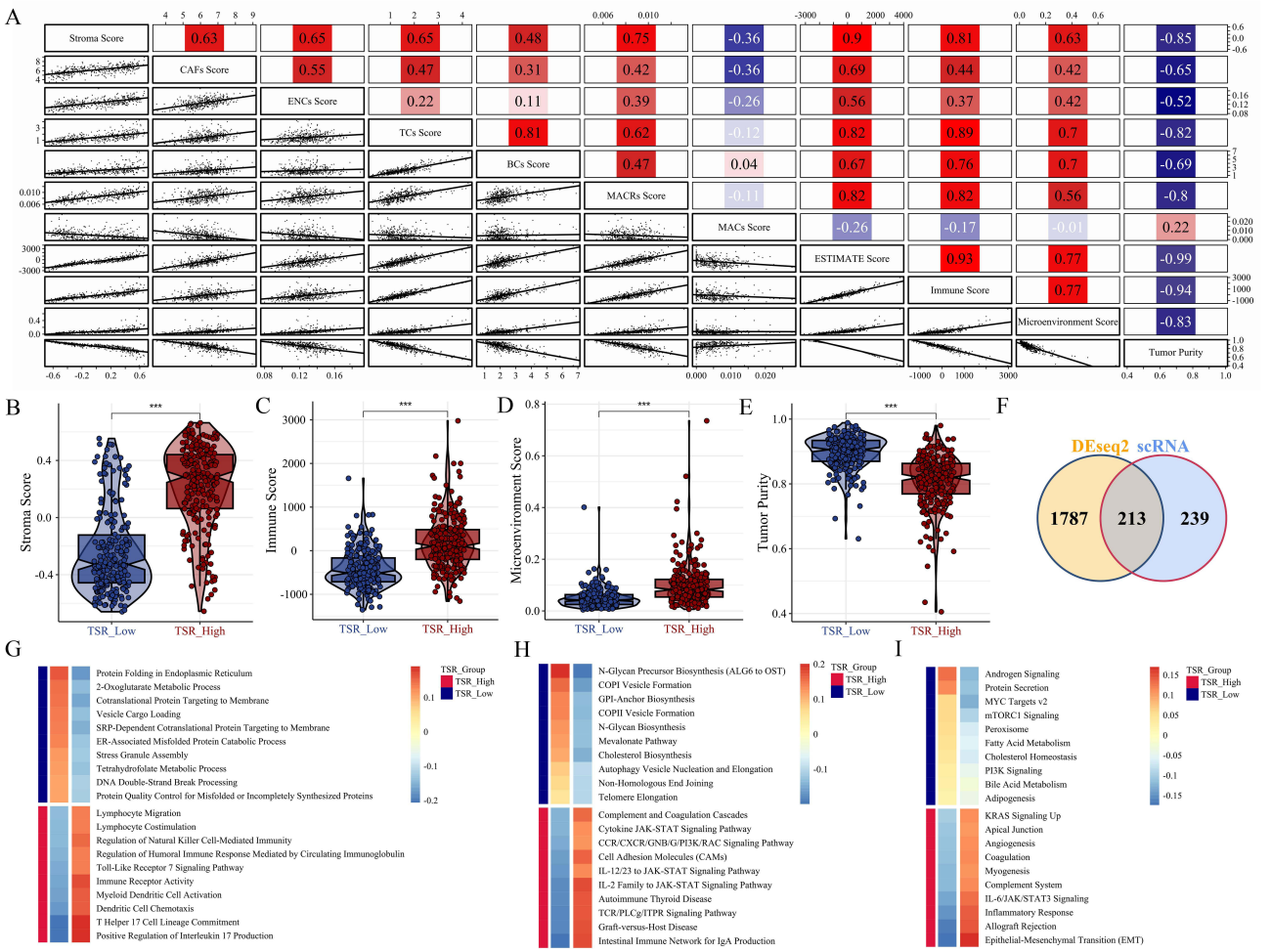

Figure 5 Identification and enrichment analysis of tumor stroma ratio (TSR)-related genes. (**A**) Spearman correlation analysis was performed to assess the association between cell subpopulation scores or stromal score, immune score, microenvironment scores. (**B**–**E**) Levels of stromal score, immune score, microenvironment score, and tumor purity in high and low TSR groups. (**F**) The Venn diagram shows the hub genes. (**G**–**I**) GSVA analysis of GO, KEGG analysis, and hallmark pathway between high and low TSR groups. ***p < 0.001.

knockdown. Subsequently, CCK-8, colony formation, cell migration, and invasion assays confirmed that BGN knockdown inhibited CAF proliferation, migration, and invasion (Figure 8D–G). Immunohistochemical staining revealed significantly higher BGN protein expression in high-TSR prostate cancer tissues compared to low-TSR tissues (Figure 8H). Conditioned media from BGN-knockdown CAFs significantly reduced DU145 cell migration compared to control conditioned media (Figure 8I). Xenograft tumors in mice injected with DU145 cells and control siRNA-transfected CAFs exhibited a significantly larger mean volume compared to those in mice injected with DU145 cells and either siBGN2- or siBGN3-transfected CAFs (Figure 8J).

To investigate the mechanism underlying the high expression of BGN in FICs, we explored whether its expression is regulated by epigenetic modifications. We demonstrated, both at the cell line and patient levels, that the high expression of BGN may be influenced by promoter methylation (Figure 8K–M).

Discussion

The prevailing view is that the tumor stroma, beyond its roles in tissue filling, physical support, and metabolic regulation, also promotes tumor malignancy.[10] Increasing evidence suggests that high TSR is an independent risk factor for poor prognosis in various solid tumors, including colorectal, bladder, and ovarian cancers.[13,14,28] Furthermore, a nearest study showed that high TSR can serve as a predictive biomarker for platinum chemotherapy resistance in ovarian carcinomas.[14] Consistent with our findings, stromal features have known prognostic significance in prostate cancer. For example,

https://doi.org/10.2147/IJGM.S515066

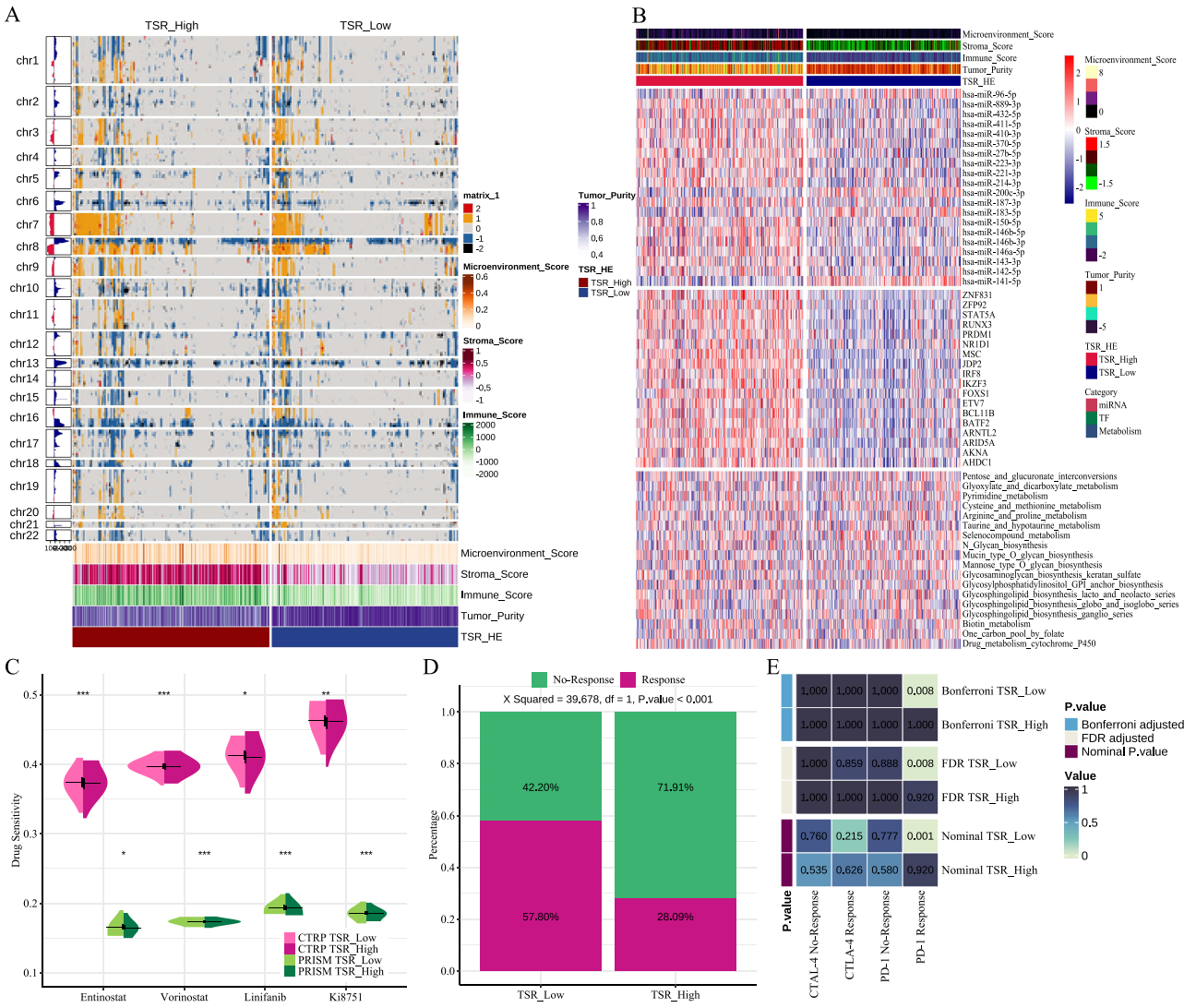

Figure 6 Tumor stroma ratio (TSR) groups differ in genomic landscape, drug sensitivity and immunotherapy response. (**A**) Genome-wide copy number landscape of 460 tumors stratified by TSR groups. Gains (gain + high balanced gain) and losses (loss + high balanced loss) are summarized to the left of the chromosome band panel. (**B**) A heatmap highlights key miRNA, transcription factor and metabolic pathway differences between high and low TSR groups. (**C**) Drug response analysis of selected agents in high and low TSR groups based on the Cancer Therapeutics Response Portal (CTRP) and Profiling Relative Inhibition Simultaneously in Mixtures (PRISM) databases. (**D**) The value of the Tumor Immune Dysfunction and Exclusion (TIDE) from The Cancer Genome Atlas (TCGA) database. (**E**) Prediction of response to anti-PD1 or anti-CTLA4 immunotherapy by submap in prostate cancer patients between high and low TSR groups. *p < 0.05, **p < 0.01, ***p < 0.001.

Yanagisawa et al (2007) showed that reactive stromal grading predicted BCR,[29] and Choi et al (2022) demonstrated that high TSR was linked to shorter BCR.[30] Our study confirmed that the TSR is an important prognostic parameter (BCR and PFI) for prostate cancer. In the TCGA cohort, after adjusting for factors such as Race and Gleason Score, multivariate Cox regression analysis revealed that high TSR remained an independent risk factor for poor prognosis (HR = 1.618, 95% CI: 1.031–2.540, $p < 0.01$). Similarly, multivariate Cox regression analysis in the LUSH cohort also indicated that high TSR remained an independent risk factor for poor prognosis (HR = 1.651, 95% CI: 1.177–2.318, $p < 0.01$). These results underscore the importance of TSR in predicting prognosis in prostate cancer patients, and its effect is independent of other known clinical factors. Further analysis confirmed that patients with high TSR exhibited significantly higher age, Gleason scores, pathologic T stage, pathologic N stage, seminal vesicle invasion, residual tumor, FPSA, and TPSA. Immunohistochemical analysis of the LUSH cohort reveals a novel complexity in the prostate cancer stromal microenvironment. Elevated AR, Ki67, PSA, and PSMA expression, coupled with decreased CK-H, p63, and Syn, suggests a pro-tumorigenic stroma. Several theories attempt to explain why high TSR within tumors may be

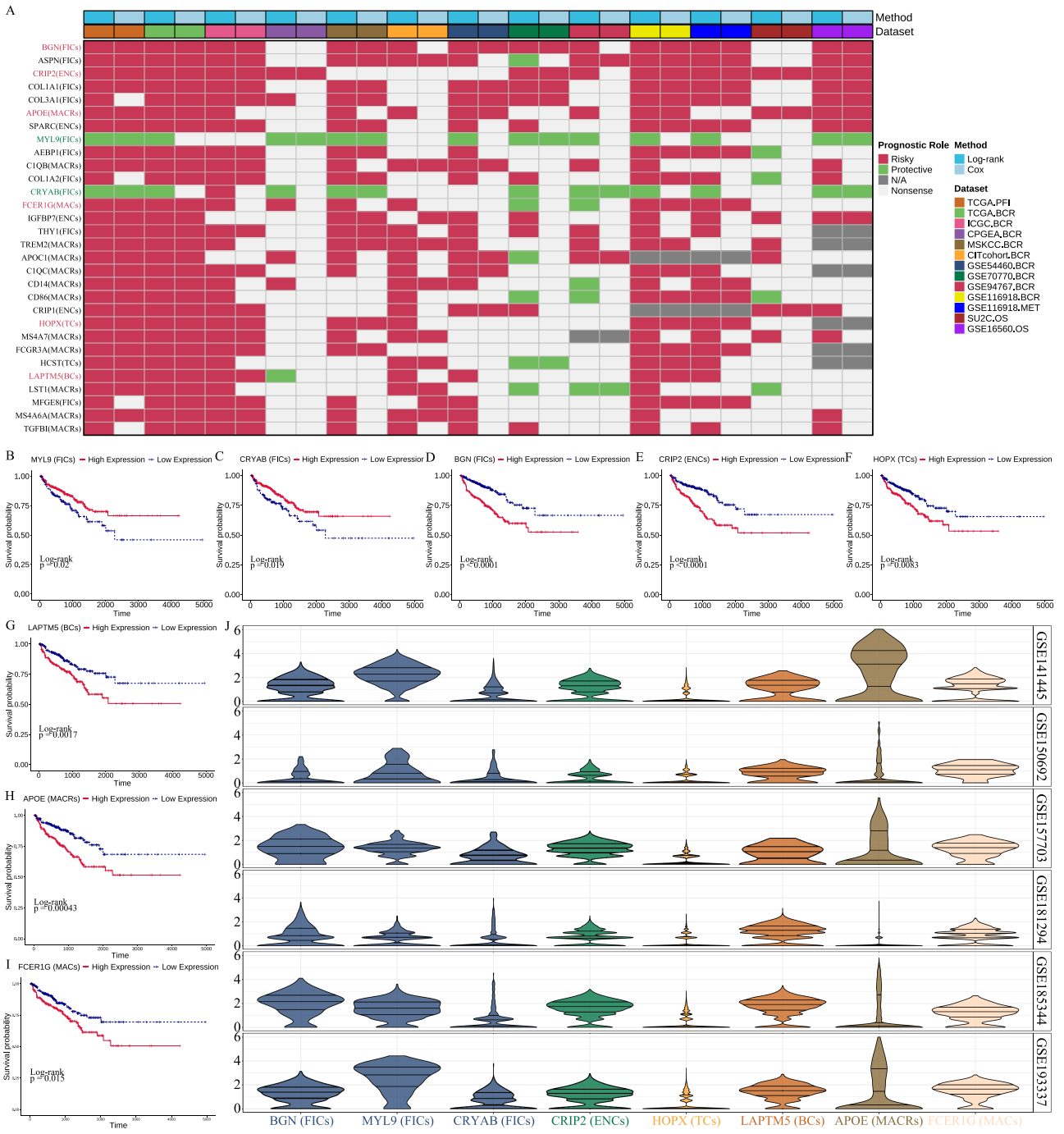

Figure 7 Prognostic impact of subgroup-associated genes was investigated. (**A**) Summary of the correlation between expression of top 30 genes with progression-free interval (PFI), biochemical recurrence (BCR), distant metastasis (MET) and overall survival (OS) based on the univariate Cox regression and Kaplan-Meier models. (**B–I**) Kaplan-Meier survival curves based on the The Cancer Genome Atlas (TCGA) dataset show the association between the expression levels of MYL9, CRYAB, BGN, CRIP2, HOPX, LAPTM5, APOE, and FCER1G genes and biochemical recurrence (BCR) in different subgroups. (**J**) The expression patterns of these genes were further analyzed in six single-cell datasets (GSE141445, GSE150692, GSE157703, GSE181294, GSE185344, GSE193337), focusing on their expression in corresponding cell subpopulations.

associated with poor prognosis. Firstly, a higher proportion of reactive stroma can produce a greater quantity of growth factors, thereby increasing the overall tumor burden.[31] Secondly, it has been suggested that high proportions of fibroblasts might contribute to reduced accessibility of the tumor to the immune response by encapsulating malignant cells and hindering their destruction.[32] In addition to TNM staging, PSA, and Gleason score, the TSR can be easily applied in routine pathology to identify patients with an increased risk of prostate cancer BCR. Therefore, incorporating

https://doi.org/10.2147/IJGM.S515066

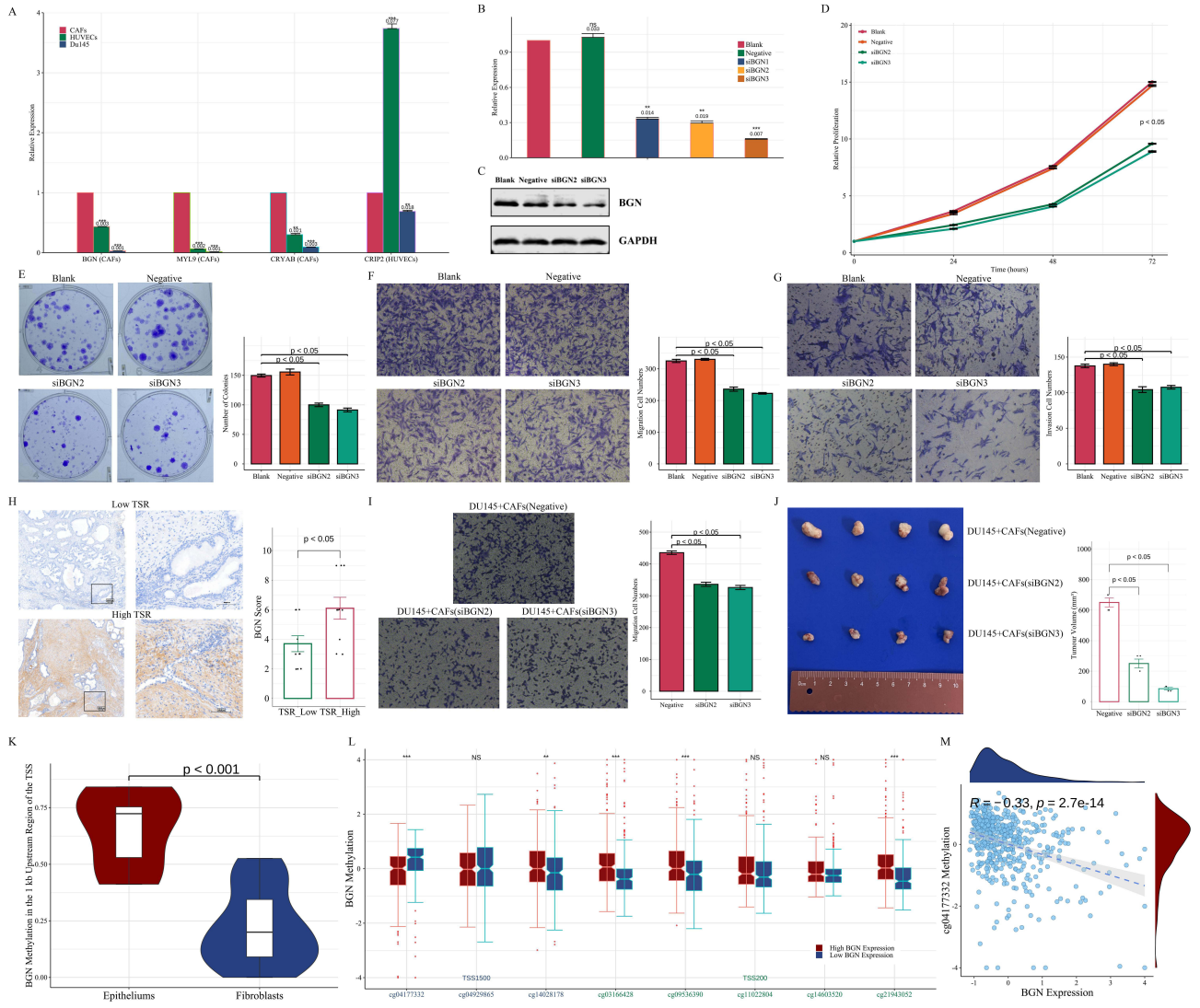

Figure 8 The function of BGN in cancer-associated fibroblasts (CAFs) and the epigenetic regulation of the BGN expression. (**A**) Validation of differentially expressed mRNAs using real-time quantitative PCR (RT-qPCR). (**B**) Fluorescence RT-qPCR detection results after siRNA transfection. (**C**) The Western blotting assay detection results after siRNA transfection. (**D–G**) Effect of BGN siRNAs on CAFs using CCK-8, colony formation, cell migration, and invasion assays. (**H**) BGN protein expression in high- and low-TSR prostate cancer tissues by immunohistochemistry. (**I**) DU145 cell migration in response to conditioned media from BGN siRNAs on CAFs. (**J**) Photographs of xenograft tumors harvested at the end of the experiment (n = 4), with tumor volumes measured for each group. (**K**) Comparing promoter methylation levels between cell line based on DepMap dataset. (**L**) Comparing promoter methylation levels between low or high BGN expression based on TCGA dataset. (**M**) Correlation between cg04177332 methylation level and mRNA expression level. **p < 0.01, ***p < 0.001.

Abbreviation: NS, not significant.

TSR assessment into routine pathology, alongside TNM staging, PSA, and Gleason score, could refine risk stratification and identify patients at higher risk of recurrence. However, the translation of TSR into clinical practice requires further validation and standardization of assessment methods. Future research should focus on developing user-friendly and cost-effective TSR assays for widespread clinical application. Furthermore, integrating TSR with genomic data will provide a more comprehensive understanding of cancer biology and enable more personalized treatment strategies.

TCGA transcriptomic data analysis revealed elevated stroma and immune scores in patients with high TSR, supporting previous findings linking TSR to tumor characteristics.[13,33] Significantly upregulated immune activation pathways and enrichment of immune-related gene sets, including TGF-β signaling and the complement system, were observed in the high TSR group.[33] Despite potential association with enhanced immune response, TIDE and SubMap algorithms indicated diminished likelihood of immunotherapy response in patients with high TSR. This seemingly paradoxical observation might be explained by the immunosuppressive effects of certain stromal components, such as

TGF-β, which is upregulated in high TSR tumors. TGF-β can promote the differentiation of regulatory T cells and inhibit the activity of cytotoxic T cells, thereby suppressing anti-tumor immunity. CNV analysis revealed an enrichment of alterations on chromosomes 3, 7, 8, and 9 in patients with high stromal content, supporting previous findings linking these CNVs to tumor progression and prognosis.[34,35] We identified specific miRNAs and transcription factors highly expressed in the high stroma group as potential therapeutic targets, given that a single miRNA or transcription factor can target multiple genes.[36] Previous studies suggest targeting miR-96-5p in fibroblasts[37] and ZNF831, a transcription factor implicated in T cell regulation in pancreatic cancer,[38] as potential therapeutic strategies for modulating the tumor microenvironment and enhancing anti-tumor immunity.

Our study identified six stromal cell-related genes: BGN, CRIP2, APOE, FCER1G, HOPX, and LAPTM5. Increased expression of these genes in fibroblasts, endothelial cells, macrophages, mast cells, T cells, and B cells, respectively, was significantly associated with poorer patient survival in prostate cancer (PCa). These findings highlight the critical role of the tumor microenvironment in disease progression. To validate our findings, we investigated the expression of BGN, MYL9, CRYAB, and CRIP2 in DU145, CAFs, and HUVECs using PCR, confirming our previous observations. Further functional studies in CAFs, using in vitro assays such as CCK-8, colony formation, cell invasion, and migration assays, demonstrated that BGN knockdown in CAFs significantly suppressed cell proliferation, migration, and invasion compared to the control group ($p < 0.05$).

BGN, an extracellular matrix protein, is known to promote tumor growth and metastasis in various cancers.[39,40] While previous studies have linked BGN to prostate cancer,[41,42] where it appears only as part of a prognostic gene set, our study uniquely demonstrates BGN's specific expression and function in CAFs. Moreover, through Log-rank and Cox analyses across multiple prostate cancer prognostic datasets, we demonstrate that BGN is an optimal prognostic marker associated with CAFs ($p < 0.05$). It's important to acknowledge that previous studies have reported more complex effects of BGN in prostate cancer. For instance, some studies have shown that BGN promotes tumor growth and metastasis by facilitating cell adhesion and invasion, and activating oncogenic pathways,[40] while others have reported that BGN can also regulate tumor microenvironment and immune response.[43] Specifically, Wu et al found that BGN expression is positively correlated with PDK1 levels in epithelial ovarian cancer.[40] In a different cancer context, Zhang et al demonstrated that BGN promotes tumor progression and the transformation of mesothelial cells into cancer-associated fibroblast-like cells in gastric cancer.[43] Consistent with our observation of higher BGN expression in fibroblasts, and in agreement with the mechanisms shown in gastric cancer, our study confirmed that BGN knockdown in CAFs significantly suppressed cell proliferation, migration, and invasion. While it is known that BGN plays a role in tumor progression and metastasis in PCa, our study provides novel insights into the tumor microenvironment by showing the critical expression of BGN specifically in CAFs and its functional impact. Our findings suggest that targeting BGN in CAFs could be a promising therapeutic strategy for prostate cancer. Future research should focus on developing BGN inhibitors or other agents that disrupt BGN signaling in CAFs, and evaluating their efficacy in preclinical models.

CRIP2, a cysteine-rich protein, has been shown to regulate cell proliferation and migration, potentially contributing to tumor progression.[44] APOE, enriched in exosomes derived from M2 macrophages, promotes tumor cell migration by activating the PI3K-AKT signaling pathway and remodeling the cytoskeleton.[45] FCER1G, a high-affinity IgE receptor, contributes to mast cell activation and degranulation, which can produce fibrosis and adhesions.[46] HOPX, a homeodomain-containing protein originally identified in cardiac development, is essential for T-cell persistence and survival, particularly in Th1 CD4 T cells upon repeated antigen stimulation.[47] LAPTM5, a lysosomal transmembrane protein, has been associated with B cell activation and proliferation, contributing to a tumor-supportive microenvironment.[48] In contrast, elevated expression of MYL9 and CRYAB in fibroblasts was associated with improved patient survival. MYL9, a myosin light chain protein, is involved in muscle contraction and cell migration.[49] CRYAB, an alpha-crystallin, acts as a molecular chaperone and rescued TGFβ1-induced fibrosis.[50] These findings suggest that specific fibroblast subtypes may play a protective role against PCa progression.

This study has several limitations, but also notable strengths. While we included both our own cohort and the TCGA dataset, the retrospective nature of the study and reliance on existing data may still limit the generalizability of the findings. Furthermore, the limited sample size, particularly for certain subgroups, may impact the statistical power of the analysis. The limited follow-up period may not be sufficient to fully assess long-term outcomes. However, these

limitations are counterbalanced by several strengths. Firstly, our study combined clinicopathological data, bulk RNA-seq, and single-cell RNA-seq to provide a comprehensive analysis of TSR in prostate cancer. Secondly, the use of digital image analysis, expert pathologist review, and various bioinformatics tools strengthens the rigor and validity of our findings. Thirdly, the inclusion of an independent validation cohort (TCGA) adds further credibility to our results. Future prospective multi-center studies with ≥500 patients, employing standardized TSR scoring protocols incorporating AI-assisted digital pathology, are needed to validate these findings. Additionally, future research should focus on investigating the impact of different treatment strategies on TSR and its relationship with clinical outcomes.

Conclusion

High TSR is identified as an independent predictor of poor prognosis in prostate cancer, offering a readily accessible parameter for risk stratification. BGN promotes CAFs malignancy, suggesting BGN inhibitors as a promising therapeutic avenue. However, further research is needed to elucidate the biological mechanisms underlying TSR-associated transcriptomic changes and to validate the clinical utility of TSR and BGN in larger, prospective cohorts, particularly in comparison to existing prognostic models.

Abbreviations

PCa, prostate cancer; PRAD, prostate adenocarcinoma; AR, Androgen receptor; CRPC, castration-resistant prostate cancer; TNM, tumor–node–metastasis; PSA, prostate-specific antigen; H&E, hematoxylin and eosin; TSR, tumor stroma ratio; OS, overall survival; buRNA-seq, bulk RNA sequencing; scRNA-seq, single-cell RNA sequencing; TCGA, The Cancer Genome Atlas; LUSH, Lanzhou University Second Hospital; TRIPOD, Transparent Reporting of a Multivariable Prediction Model for Individual Prognosis or Diagnosis; pT, pathologic T stage; pN, pathologic N stage; BCR, biochemical recurrence; PFI, progression-free interval; BMI, body mass index; FPSA, free prostate-specific antigen; TPSA, total prostate-specific antigen; WBC, white blood cell; RBC, red blood cell; ELR, eosinophil-to-lymphocyte ratio; BLR, basophil-to-lymphocyte ratio; NLR, neutrophil-to-lymphocyte; MLR, monocyte-to-lymphocyte ratio; PCA, principal component analysis; UMAP, uniform manifold approximation and projection; DEGs, differentially expressed genes; ICGC, International Cancer Genome Consortium; GSEA, gene set enrichment analysis; CTRP, Cancer Therapeutics Response Portal; PRISM, Profiling Relative Inhibition Simultaneously in Mixtures; TIDE, Tumor Immune Dysfunction and Exclusion; HUVECs, human umbilical vein endothelial cells; qRT-PCR, quantitative Real-time quantitative PCR; CCK-8, Cell Counting Kit-8.

Data Sharing Statement

The datasets used and/or analyzed during the current study are available from the corresponding author upon reasonable request.

Ethics Approval

This study was approved by the Ethics Committee of Lanzhou University Second Hospital.

Informed Consent Statement

All participants signed a free and informed consent statement.

Acknowledgments

The authors gratefully acknowledge the public data of TCGA and GEO datasets.

Disclosure

The authors declare that they have no competing interests in this work.

References

1. Bray F, Laversanne M, Sung H, et al. Global cancer statistics 2022: GLOBOCAN estimates of incidence and mortality worldwide for 36 cancers in 185 countries. *CA Cancer J Clin*. 2024;74(3):229–263. doi:10.3322/caac.21834
2. Gandaglia G, Leni R, Bray F, et al. Epidemiology and Prevention of Prostate Cancer. *Eur Urol Oncol*. 2021;4(6):877–892. doi:10.1016/j.euo.2021.09.006
3. Al Olama AA, Kote-Jarai Z, Berndt SI, et al. A meta-analysis of 87,040 individuals identifies 23 new susceptibility loci for prostate cancer. *Nat Genet*. 2014;46(10):1103–1109. doi:10.1038/ng.3094
4. Wang ZA, Mitrofanova A, Bergren SK, et al. Lineage analysis of basal epithelial cells reveals their unexpected plasticity and supports a cell-of-origin model for prostate cancer heterogeneity. *Nat Cell Biol*. 2013;15(3):274–283. doi:10.1038/ncb2697
5. Spratt DE, Zumsteg ZS, Feng FY, Tomlins SA. Translational and clinical implications of the genetic landscape of prostate cancer. *Nat Rev Clin Oncol*. 2016;13(10):597–610. doi:10.1038/nrclinonc.2016.76
6. Cai M, Song XL, Li XA, et al. Current therapy and drug resistance in metastatic castration-resistant prostate cancer. *Drug Resist Updat*. 2023;68:100962. doi:10.1016/j.drup.2023.100962
7. Ge Q, Li J, Yang F, et al. Molecular classifications of prostate cancer: basis for individualized risk stratification and precision therapy. *Ann Med*. 2023;55(2):2279235. doi:10.1080/07853890.2023.2279235
8. Chung LW, Baseman A, Assikis V, Zhau HE. Molecular insights into prostate cancer progression: the missing link of tumor microenvironment. *J Urol*. 2005;173(1):10–20. doi:10.1097/01.ju.0000141582.15218.10
9. Tyekucheva S, Bowden M, Bango C, et al. Stromal and epithelial transcriptional map of initiation progression and metastatic potential of human prostate cancer. *Nat Commun*. 2017;8(1):420. doi:10.1038/s41467-017-00460-4
10. Valkenburg KC, de Groot AE, Pienta KJ. Targeting the tumour stroma to improve cancer therapy. *Nat Rev Clin Oncol*. 2018;15(6):366–381. doi:10.1038/s41571-018-0007-1
11. Mesker WE, Junggeburt JM, Szuhai K, et al. The carcinoma-stromal ratio of colon carcinoma is an independent factor for survival compared to lymph node status and tumor stage. *Cell Oncol*. 2007;29(5):387–398. doi:10.1155/2007/175276
12. He R, Li D, Liu B, et al. The prognostic value of tumor-stromal ratio combined with TNM staging system in esophagus squamous cell carcinoma. *J Cancer*. 2021;12(4):1105–1114. doi:10.7150/jca.50439
13. Liu J, Li C, Huang K, et al. A classification based on tumor-stroma ratio and tumor budding for patients with muscle-invasive bladder cancer. *Expert Rev Anticancer Ther*. 2022;22(3):323–330. doi:10.1080/14737140.2022.2012158
14. Lou E, Clemente V, Grube M, et al. Tumor-Stroma Proportion to Predict Chemoresistance in Patients With Ovarian Cancer. *JAMA Network Open*. 2024;7(2):e240407. doi:10.1001/jamanetworkopen.2024.0407
15. Wu J, Liang C, Chen M, Su W. Association between tumor-stroma ratio and prognosis in solid tumor patients: a systematic review and meta-analysis. *Oncotarget*. 2016;7(42):68954–68965. doi:10.18632/oncotarget.12135
16. Moons KG, Altman DG, Reitsma JB, et al. Transparent Reporting of a multivariable prediction model for Individual Prognosis or Diagnosis (TRIPOD): explanation and elaboration. *Ann Intern Med*. 2015;162(1):W1–73. doi:10.7326/m14-0698
17. World Medical Association. Declaration of Helsinki: ethical principles for medical research involving human subjects. *JAMA*. 2013;310(20):2191–2194. doi:10.1001/jama.2013.281053.
18. Qin X, Han C, Zhang H, et al. Outcomes of patients with lymph node metastasis treated with radical prostatectomy and adjuvant androgen deprivation therapy in a Chinese population: results from a cohort study. *World J Surg Oncol*. 2015;13(1):172. doi:10.1186/s12957-015-0597-3
19. Lou E, Vogel RI, Hoostal S, et al. Tumor-Stroma Proportion as a Predictive Biomarker of Resistance to Platinum-Based Chemotherapy in Patients With Ovarian Cancer. *JAMA Oncol*. 2019;5(8):1222–1224. doi:10.1001/jamaoncol.2019.1943
20. Chen Y, Zhang L, Liu W, Liu X. Prognostic Significance of the Tumor-Stroma Ratio in Epithelial Ovarian Cancer. *Biomed Res Int*. 2015;2015:589301. doi:10.1155/2015/589301
21. Chen S, Zhu G, Yang Y, et al. Single-cell analysis reveals transcriptomic remodellings in distinct cell types that contribute to human prostate cancer progression. *Nat Cell Biol*. 2021;23(1):87–98. doi:10.1038/s41556-020-00613-6
22. Crowley L, Cambuli F, Aparicio L, et al. A single-cell atlas of the mouse and human prostate reveals heterogeneity and conservation of epithelial progenitors. *Elife*. 2020;9:59465. doi:10.7554/eLife.59465
23. Ma X, Guo J, Liu K, et al. Identification of a distinct luminal subgroup diagnosing and stratifying early stage prostate cancer by tissue-based single-cell RNA sequencing. *Mol Cancer*. 2020;19(1):147. doi:10.1186/s12943-020-01264-9
24. Hirz T, Mei S, Sarkar H, et al. Dissecting the immune suppressive human prostate tumor microenvironment via integrated single-cell and spatial transcriptomic analyses. *Nat Commun*. 2023;14(1):663. doi:10.1038/s41467-023-36325-2
25. Wong HY, Sheng Q, Hesterberg AB, et al. Single cell analysis of cribriform prostate cancer reveals cell intrinsic and tumor microenvironmental pathways of aggressive disease. *Nat Commun*. 2022;13(1):6036. doi:10.1038/s41467-022-33780-1
26. Heidegger I, Fotakis G, Offermann A, et al. Comprehensive characterization of the prostate tumor microenvironment identifies CXCR4/CXCL12 crosstalk as a novel antiangiogenic therapeutic target in prostate cancer. *Mol Cancer*. 2022;21(1):132. doi:10.1186/s12943-022-01597-7
27. Zhan S, Liu Z, Zhang M, et al. Overexpression of B7-H3 in α-SMA-Positive Fibroblasts Is Associated With Cancer Progression and Survival in Gastric Adenocarcinomas. *Front Oncol*. 2019;9:1466. doi:10.3389/fonc.2019.01466
28. West NP, Dattani M, McShane P, et al. The proportion of tumour cells is an independent predictor for survival in colorectal cancer patients. *Br J Cancer*. 2010;102(10):1519–1523. doi:10.1038/sj.bjc.6605674
29. Yanagisawa N, Li R, Rowley D, et al. Stromogenic prostatic carcinoma pattern (carcinomas with reactive stromal grade 3) in needle biopsies predicts biochemical recurrence-free survival in patients after radical prostatectomy. *Hum Pathol*. 2007;38(11):1611–1620. doi:10.1016/j.humpath.2007.04.008
30. Choi JB, Han KH, Lee Y, et al. The incidence of testicular torsion and testicular salvage rate in Korea over 10 years: a nationwide population-based study. *Investig Clin Urol*. 2022;63(4):448–454. doi:10.4111/icu.20220122
31. Levesque C, Nelson PS. Cellular Constituents of the Prostate Stroma: key Contributors to Prostate Cancer Progression and Therapy Resistance. *Cold Spring Harb Perspect Med*. 2018;8(8):30510. doi:10.1101/cshperspect.a030510

32. Bonollo F, Thalmann GN, Kruithof-de Julio M, Karkampouna S. The Role of Cancer-Associated Fibroblasts in Prostate Cancer Tumorigenesis. *Cancers*. 2020;12(7):1887. doi:10.3390/cancers12071887
33. Ravensbergen CJ, Kuruc M, Polack M, et al. The Stroma Liquid Biopsy Panel Contains a Stromal-Epithelial Gene Signature Ratio That Is Associated with the Histologic Tumor-Stroma Ratio and Predicts Survival in Colon Cancer. *Cancers*. 2021;14(1):163. doi:10.3390/cancers14010163
34. Feuk L, Carson AR, Scherer SW. Structural variation in the human genome. *Nat Rev Genet*. 2006;7(2):85–97. doi:10.1038/nrg1767
35. Frank B, Bermejo JL, Hemminki K, et al. Copy number variant in the candidate tumor suppressor gene MTUS1 and familial breast cancer risk. *Carcinogenesis*. 2007;28(7):1442–1445. doi:10.1093/carcin/bgm033
36. Arora S, Rana R, Chhabra A, Jaiswal A, Rani V. miRNA-transcription factor interactions: a combinatorial regulation of gene expression. *Mol Genet Genomics*. 2013;288(3–4):77–87. doi:10.1007/s00438-013-0734-z
37. Xu W, Liu S, Ma L, et al. Identification of miRNA signature in cancer-associated fibroblast to predict recurrent prostate cancer. *Comput Biol Med*. 2024;180:108989. doi:10.1016/j.compbiomed.2024.108989
38. Tan Z, Lei Y, Zhang B, et al. Analysis of Immune-Related Signatures Related to CD4+ T Cell Infiltration With Gene Co-Expression Network in Pancreatic Adenocarcinoma. *Front Oncol*. 2021;11:674897. doi:10.3389/fonc.2021.674897
39. Zheng S, Liang JY, Tang Y, et al. Dissecting the role of cancer-associated fibroblast-derived biglycan as a potential therapeutic target in immunotherapy resistance: a tumor bulk and single-cell transcriptomic study. *Clin Transl Med*. 2023;13(2):e1189. doi:10.1002/ctm2.1189
40. Wu H, Xiang Z, Huang G, et al. BGN/FAP/STAT3 positive feedback loop mediated mutual interaction between tumor cells and mesothelial cells contributes to peritoneal metastasis of gastric cancer. *Int J Biol Sci*. 2023;19(2):465–483. doi:10.7150/ijbs.72218
41. Liu W, Wang M, Wang M, Liu M. Single-cell and bulk RNA sequencing reveal cancer-associated fibroblast heterogeneity and a prognostic signature in prostate cancer. *Medicine*. 2023;102(32):e34611. doi:10.1097/md.0000000000034611
42. Bettin A, Reyes I, Reyes N. Gene expression profiling of prostate cancer-associated genes identifies fibromodulin as potential novel biomarker for prostate cancer. *Int J Biol Markers*. 2016;31(2):e153–62. doi:10.5301/jbm.5000184
43. Zhang L, Yan L, Fu X, et al. PDK1 promotes epithelial ovarian cancer progression by upregulating BGN. *Acta Biochim Biophys Sin*. 2024. doi:10.3724/abbs.2024186
44. Billhaq DH, Lee SH, Lee S. The potential function of endometrial-secreted factors for endometrium remodeling during the estrous cycle. *Anim Sci J*. 2020;91(1):e13333. doi:10.1111/asj.13333
45. Zheng P, Luo Q, Wang W, et al. Tumor-associated macrophages-derived exosomes promote the migration of gastric cancer cells by transfer of functional Apolipoprotein E. *Cell Death Dis*. 2018;9(4):434. doi:10.1038/s41419-018-0465-5
46. Konno R, Yamada-Okabe H, Fujiwara H, et al. Role of immunoreactions and mast cells in pathogenesis of human endometriosis--morphologic study and gene expression analysis. *Hum Cell*. 2003;16(3):141–149. doi:10.1111/j.1749-0774.2003.tb00146.x
47. Zheng C, Fass JN, Shih YP, et al. Transcriptomic profiles of neoantigen-reactive T cells in human gastrointestinal cancers. *Cancer Cell*. 2022;40(4):410–423.e7. doi:10.1016/j.ccell.2022.03.005
48. Glowacka WK, Alberts P, Ouchida R, Wang JY, Rotin D. LAPTM5 protein is a positive regulator of proinflammatory signaling pathways in macrophages. *J Biol Chem*. 2012;287(33):27691–27702. doi:10.1074/jbc.M112.355917
49. Licht AH, Nübel T, Feldner A, et al. Junb regulates arterial contraction capacity, cellular contractility, and motility via its target Myl9 in mice. *J Clin Invest*. 2010;120(7):2307–2318. doi:10.1172/jci41749
50. Cheng L, Zou X, Wang J, Zhang J, Mo Z, Huang H. The role of CRYAB in tumor prognosis and immune infiltration: a Pan-cancer analysis. *Front Surg*. 2022;9:1117307. doi:10.3389/fsurg.2022.1117307